IJME

*Int. J. of Applied Mechanics and Engineering, 2026, vol.31, No.1, pp.1-15*
DOI: 10.59441/ijame/214978

# CENTRAL HOLE SIZE INFLUENCES A FATIGUE CRACK BEHAVIOR OF Al7050-T6 ALLOY

M.A.N. Ali[1*], L.K. Jawad[2] and A.I. Razooqi[1]
[1]Applied Mechanics Technical Engineering Department, Middle Technical University/ Technical Engineering College-Baghdad, IRAQ
[2]Materials Technical Engineering Department, Middle Technical University/ Technical Engineering College-Baghdad, IRAQ
E-mail: maaltememy69@yahoo.com

This research studied experimentally the behavior of an aluminum alloy 7050 thin plate containing different sizes of circular central holes under thermo-mechanical fatigue crack growth testing. Transient thermal cyclic loading from *50°C* to where applied, combined with constant tensile mechanical load at *200 kg* at the edge of the plate. Three cases were experimentally tested based on the hole diameter of (*1, 2*, *3 mm*) under the same testing conditions. Results show the increment of central hole diameter makes the crack initiation start earlier and crack growth increases then goes faster. Also, it has increased the stress intensity. The length of the second region of crack propagation related to stress intensity decreased when the hole size increased, and the slope changed too. For that, different Paris laws were obtained based on the central hole size. Accordingly, to these Paris laws, it can be easily informed and analyzed the behavior of any engineering structure made of this type of alloy under the same loading condition and predict its fracture or failure limits or lives.

**Key words:** aluminum 7050-T6, circular central hole sizes, cyclic thermal shock, and experimental thermo-mechanical testing.

## 1. Introduction

Presently, one of the topics in scientific subjects in many industries dealing with high temperature loading on the engineering designer is the thermo-mechanical fatigue behavior and resistance of the selected element or part material. Many industrial sectors such as internal combustion engines, boilers, turbojet engines, and classical and nuclear power plant components all operate with components subjected to transient high temperatures combined with mechanical stresses due to their developing performance requirements. These components could have failed because of thermal or thermo-mechanical fatigue failures. Thermal fatigue is the consequence of cyclic stresses induced by temperature changes, whereas thermo-mechanical fatigue is the superimpose of thermal stress with mechanical stress. While thermal shock cycling is a varying temperature applied to the component in a short period of time that creates a temperature gradient and causes the component to endure severe thermal stresses. It is one of the forms of thermal fatigue cycling.

Failure may occur when the resulting combined thermo-mechanical stress exceeds the material's strength in that way of stressing. One of the main reasons of early failure or crack initiation due to large variation in temperature within a short range of time is the difficulty of material prediction which can be well chosen for its performance under that transient thermo-mechanical cyclic loading, Ali *et al.* [1], Garden [2]. It is necessary to provide the most reliable components in the automotive industry to the customers in a very competitive market. According to the performance and ecological considerations, engines tend to be exposed to higher temperatures and pressures during their normal operation. So that, makes the selection of a design and an associated material for an engine part should be accurate in the early conception stages, moreover, the

* To whom correspondence should be addressed

design engineers should have get at an efficient experimental basis, that quickly assess the alternative geometries, materials and production processes, Szmytka *et al.* [3].

The crack or defects or cavities or hole size have a crucial impact on the strength behavior of the materials during real-life applications. This is reflected in the designed engineering components, especially those subjected to combined cyclic thermo-mechanical loading. This crack or hole size is taken as a size to width ratio that cannot be greater than *30%*, because a larger ratio (crack or hole size) increases the stress intensity and speeds up the crack propagation according to linear elastic fracture mechanics concepts, which is the main method that this study deals with. These are clearly illustrated in the turbine blades of aerospace, airplane, and power generation engines that are subjected to centrifugal force as a mechanical load combined with thermal variation during startup and shutdown operations. Also occurred in the automotive internal combustion engine components such as cylinder head, piston, connecting rods, and also the exhaust manifold that were subjected to fuel explosion pressure as a mechanical load combined with temperature gradients of the existing gases during starting and shutting off the car engine. Similarly, occurred in the rocket nozzles and its combustion chamber and boilers that were subjected to the combination of internal pressure and the variation of the exhaust gases or steam temperatures.

Aluminum alloy Al7050-Ti was a major alloying element utilized in a variety of manufacturing and construction applications of industries that needed high strength and fatigue resistance for several decades. It is a metal matrix composite with hybrid reinforcement containing superior properties of high strength, stiffness, hardness, surface roughness, wear resistance, and lightweight. It is applicable in the automotive engines and other internal combustion components like pistons, cylinders, connecting rods, and cylinder sleeve, also in the brake parts such as impellers, guide vanes, rotating shafts, space shuttles. Moreover, in robots, armour, and aircraft components. The properties of heat treated aluminum alloy Al7050 were developed by adding many additives such as hybrid reinforcements of Ti, Si/SiC, and graphene. Titanium additive is the commonly reinforcement added to the aluminum, mostly added in the form of nanoparticles to Al7050, Muthukumaran *et al.* [4].

Under the knowledge of the author, there aren't any research efforts or works involved in the thermo-mechanical fatigue investigation on the Al7050 alloy for twenty-fifth years ago. The literature reviews presented in this research are for thermal or mechanical fatigue investigations and their combination of the same group of aluminum alloy Al7xxx or other groups focusing on different characteristics influences. For the Al7xxx group, the researcher presented an investigation of high temperature fatigue behaviour for Al7075 under different mechanical and heat treatment procedures. Experimental cyclic bending fatigue tests were adopted for room temperatures, *250* and *300℃*. A surface enhancement application called low plasticity burnishing was utilized for testing specimens to improve their fatigue resistance and also analyzed its effect on the fatigue behaviour of the material under high temperatures. Results show that the burnishing process highly increased the fatigue stiffness of the surface and delayed the fatigue crack initiation. Moreover, increasing the temperature lowered the fatigue lives, and the machined specimens have longer lives in comparison with the heat treatment specimens, which causes a degradation of fatigue resistance. In addition, found that surface enhancement decreased the oxidation effect during the high temperature fatigue due to the plasticity undergoing through the crack growth indicated by intense striations, Abo El-Nasr *et al.* [5]. Lots of researchers found the importance of minimizing the fatigue resistance of 2xxx and 7xxx aluminium alloys compared to the reference type because of the state of the machined and polished surface of the material. Explaining that decrease was related to the porosity and the oxide layer behavior of the material, in addition to the tensile residual stresses that occurred at the interface between the oxide layer and the substrate. This was demonstrated by an experimental bending fatigue investigation at room temperature on 7050-T7651 chromic acid anodized aluminium alloy in order to formulate a predictive fatigue life model that deals with different characteristics of experimental fatigue crack propagation. Four point bending tests were adopted for different specimens to study the effects of the machined, pickled, and anodized process on the fatigue resistance. The observations show that, pickling process was the most decrease fatigue resistance process due to crack initiation responsibility, then comes the anodizing process, Chaussumier, *et al.* [6].

For other types of aluminum widely used in the fabrication of car cylinder heads, researchers studied the high thermal fatigue behavior at room and elevated temperatures for three types of cast aluminum alloys:

319, A356, and AS7GU. Out-of-phase and in-phase thermo-mechanical fatigue behavior investigation was adopted under loading conditions (*100-300°C*). This research aimed to make a comparison between the high cycle, low cycle and thermo-mechanical fatigue behaviors of these cast aluminum alloys under different heat treatments to study their actual treatment reflection during production. Results show that the alloys demonstrated similar behaviors under isothermal and thermo-mechanical low-cycle fatigue analysis. While, during the high-cyclic fatigue the alloys A356 and AS7GU presented better strength and fatigue performances, Carlos *et al.* [7]. Other researchers took these types of alloys (319 and 356) under consideration through a comparative investigation of the out-of-phase thermo-mechanical fatigue (TMF) behavior under temperature cycling (*60-300°C*) and different strain rates (*0.1-0.6%*), focusing on the evaluation of the relationship between the micro-structure. Found that the two types of aluminum alloys have asymmetrical hysteresis loops and higher tensile mode than compression during TMF cycling testing. Regarding maximum stress, both alloys exhibit a cyclic softening behavior, but the reduction in the cyclic stress rate in the 356 alloy was earlier at higher strain amplitudes. Also, results show that the thermal fatigue life of 319 alloy was longer than 356 alloy during high strain rates. This was related to the coarsening of (-MgSi in 356 and $Al_2Cu$ in 319) precipitates during the TMF tests; however, the rate of precipitates changing per cycle in the 356 alloy was significantly greater. Moreover, the model was adopted to predict the fatigue based on energy possessed low fatigue damage capacity and high fatigue damage exponent, Liu *et al.* [8].

For aluminum Al2024 type, researchers focused on studying the improvements of this type through studying the impact of using $TiO_2$ nanoparticles on the fatigue behaviour of AA2024 before and after heat treatment. The optimum enhancement was adopted at 5 wt. *%* $TiO_2$ after heat treatment, and the fatigue life was investigated experimentally and numerically. Results show there was a good match of *4%* between the experimental results and numerical fatigue measurement with an improvement of fatigue life of *14.71%* in comparison with the based sample. The highest fatigue strength was exhibited under constant amplitude loads reaching to *82 MPa* at 107 cycles. This is related to the increment of fine precipitations besides its uniform distribution after the heat treatment. The SEM analysis of the heat treatment and aging process of AA2024 with $TiO_2$ nanocomposite gives a fair distribution of fine grains in comparison to the metal matrix, Hamid *et al.* [9]. Also, another thermo-mechanical fatigue strength study was presented to examine the effect of load temperature combination on the surface crack propagation of 2024 T3 aluminum alloy. Numerical modelling was adopted using ABAQUS to study the fatigue crack propagation life and predict the initiation of fatigue damage components. Results show that the load ratio effect was shifting the crack growth rate curve. Moreover, using appropriate thermo-mechanical behavior laws in different phases gives an important role due to the residual stress distribution. While the temperature increment increases the equivalent stresses, axial displacements, and total deformation. Finally, the temperature influence on crack propagation presented the best lifetime prediction, where the damage clearly detected within higher temperature, Abdallah *et al.* [10].

For the aluminium alloy AA6061 fatigue life behaviour, many analytical approaches were adopted to consider the fatigue life behaviour at high temperatures. A finite element analysis for the stress-life behaviours at different temperatures (*50*, *100*, *150*, *200*, *250*, and *300℃*) was measured by linear interpolation. Where Basquin relation is used as a good alternative approach for the fatigue life prediction at high temperatures without much experimental analysis taken into consideration. Results show that the number of cycles till failure was significantly influenced by temperature. Through observing, the failure fatigue life was reduced by *99%* at *300℃*. According to the high temperature fatigue influence, this research discovered that aluminium alloy AA6061 was unsuitable for most of the automotive engine parts, Hussain *et al.* [11]. Also, the thermal fatigue behaviour of Aluminum alloy (A-6063) was investigated experimentally under rotating bending with a stress ratio $R = -1$ and varying temperatures. Found that high temperatures reduced the failure fatigue lives with increasing the temperature according to a power law. Moreover, the measured fatigue damage at high temperature was greater than the experimental damage at room temperature. This increase in damage ratio is due to the increment of the cyclic ratio at higher temperatures. At *150℃*, the fatigue life reduction was about *23%* and the fatigue endurance limit was reduced by *5.23%*. This gives that the effect of the thermal-fatigue should be taken under consideration during all design and application stages because the high temperature will faster the failure due to damage accumulation, Kadhim *et al.* [12].

This present work is aimed at experimentally discovering the fatigue crack growth behavior of an aluminum alloy 7075-T6 thin plate within different central hole sizes under thermal shock cycling combined with constant mechanical load.

## 2. Testing rig

The testing rig is designed with specifications that can produce thermal shock consisting of transient heating and cooling combined with static mechanical loading. This rig has the capability to record the distribution of temperature with a time along the specimen surface. The rig design can give the desired results with a good duration of metal breakage at a low cost, and it could be available in different materials, temperatures, and mechanical loading. The real and design layout of the testing rig consists of different measuring equipment as shown in Fig.1. The testing rig is constructed into a rig structure, weight scale, electronic control system, electric heaters, and air blower. The rig structure is made of steel frame with *1.5 m* length and *0.5 m* width. A screw of *0.4 m* long is used to connect the load scale with the traverse beam at the lower rig frame. A base is welded to the frame to fix the air blower; also two fixtures are used to secure fastening the sample from their edges. One is welded on the top of the frame, and the second is connected to the load scale. Two heaters with four small discs of ceramic used as an electrical insulation all are fixed on the rig frame by bases.

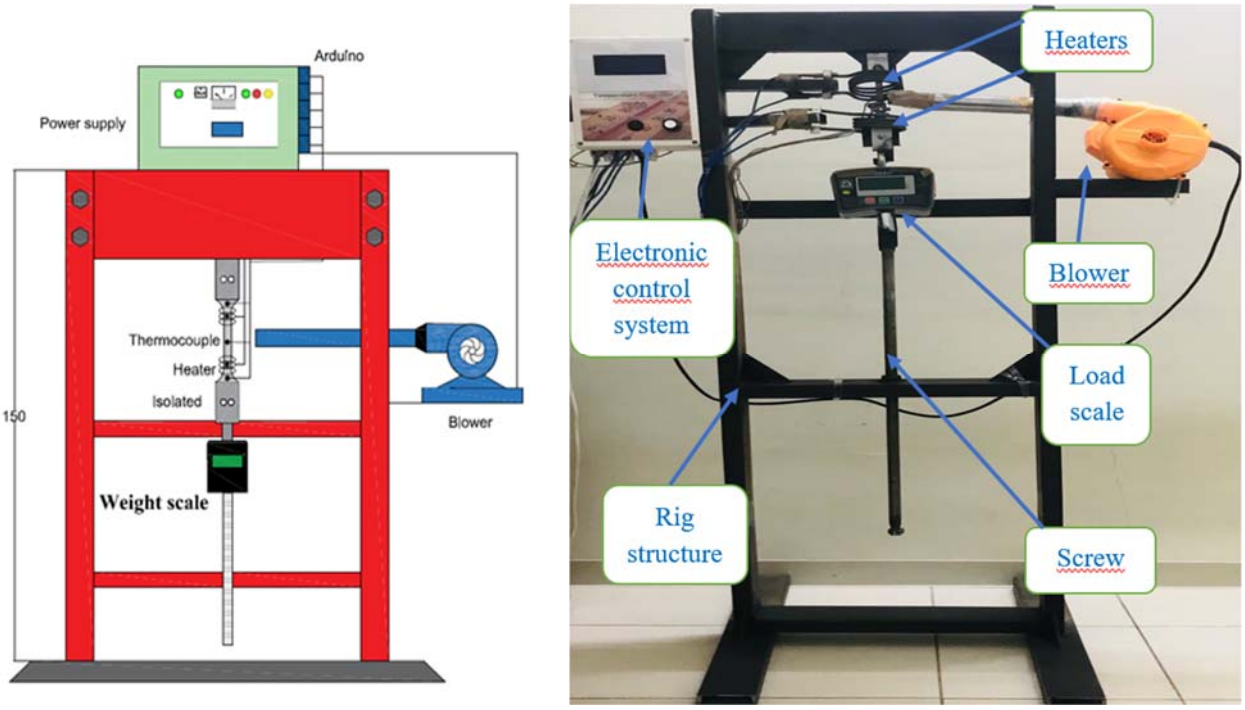


Fig.1. The design layout and real testing rig.

The heating process during the experimental work is done by using two types of heaters inserted inside a copper tube with a diameter of *7 mm* and *270 mm*, long, made with four turns, giving a power of *1000* watts. While the cooling process is done by an air blower type INGCO. The mechanical loading is obtained by using a weighing scale model (cs300 ecco), its accuracy (*0.2*), and capacity (*500 kg*), which is connected to the long screw and testing specimen. Thermometer sensor type (MAX6675) was used having an accuracy of *±0.1°C*, resolution of *0.1°C* of full-scale division for temperature range (*0* to *1024°C*) built in the electronic control circuit connected with thermocouples type K, all are shown in Fig.1. Due to the testing rig involved within many sensitive components, it should be taken great importance to calibrate these components correctly, and

to confirm there aren't any errors occurring during the testing operation, calculations, and recorded results related to the experimental values. The main and important rig parts consisted of the six k-type thermocouples, load scale, heaters, and Arduino that were calibrated under standard procedures in the Central Organization for Standardization and Quality Control in Baghdad, Iraq.

## 3. Temperature measurement

During the down shock, the sample is subjected to transient cooling, so the distribution of the temperature measurement along the sample surface was made by six thermocouples type K located in different locations on the sample as shown in Fig.2A, and the location diagram is shown in Fig.2B.

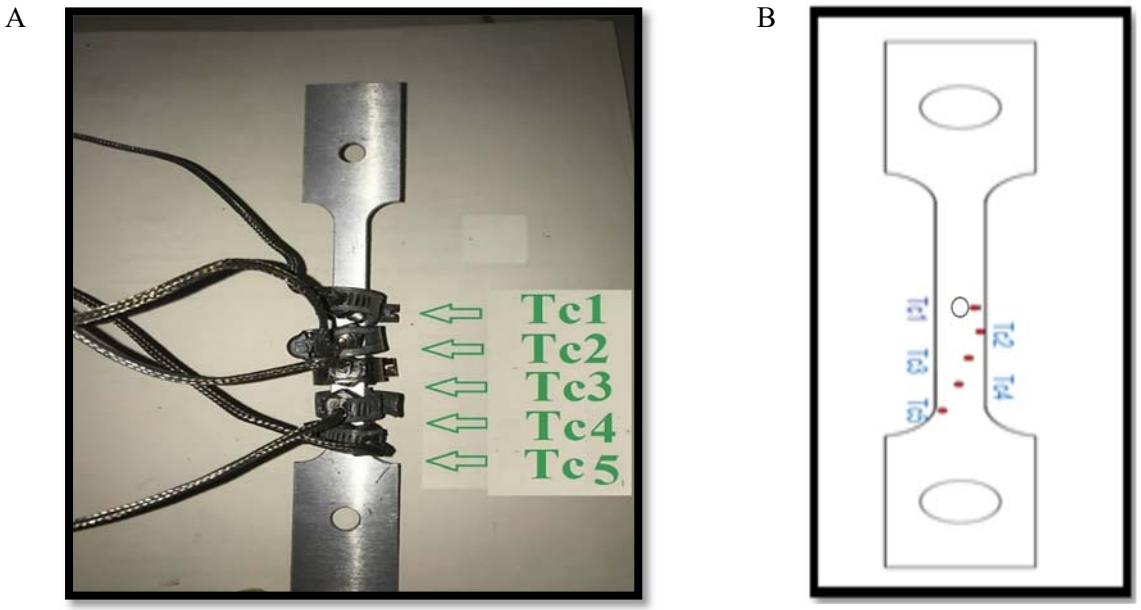


Fig.2. The distribution of thermocouple locations.

## 4. Material and testing specifications

In this work, the selected material was an aluminum alloy 7050-T6. This alloy is mostly employed in the manufacturing of automotive engine parts that are subjected to thermo-mechanical loading, which is the main issue of this present work. The metallurgical investigation of the used material was tested by a chemical composition test to confirm the correct selection of the material. Thin plate with dimensions of $(200\times10\times1)$ samples were tested in the Central Agency for Measurement and Quality Control, where the results are shown in Tab.1.

Table 1. The chemical composition of the selected material.

| Sample | Si | Fe | Cu | Mn | Mg | Zn | Cr | Ni | Pb | Ti | P | Al |
|---|---|---|---|---|---|---|---|---|---|---|---|---|
| *%* | *0.583* | *0.447* | *0.254* | *0.0575* | *0.976* | *0.0534* | *0.209* | *0.0068* | *0.018* | *0.0222* | *0.001* | *97.4* |

Tensile tests were conducted to obtain the mechanical properties of the selected material. The tests were carried out on three specimens cut from the main sheet of raw material. The alloy samples were tested in the Central Agency for Measurement and Quality Control as shown in Tab.2.

Table 2. The average mechanical property specification of the selected material.

| Sample | Ultimate stress $(\sigma_u)$ $\left(N/mm^2\right)$ | Yield strength $(\sigma_y)$ $\left(N/mm^2\right)$ | Modulus of elasticity $(GPa)$ | Elongation % | Poison's ratio |
|---|---|---|---|---|---|
| Plate $(th=1mm)$ | *360* | *325* | *73.3* | *15* | *0.33* |

The sample model is an (I) shape with different central circular hole sizes of (*1*, *2*, and *3 mm*) diameter, where the design and manufactured samples are shown in Fig.3. These samples were manufactured by using a CNC machine to cut the designed shape of the main alloy plate.

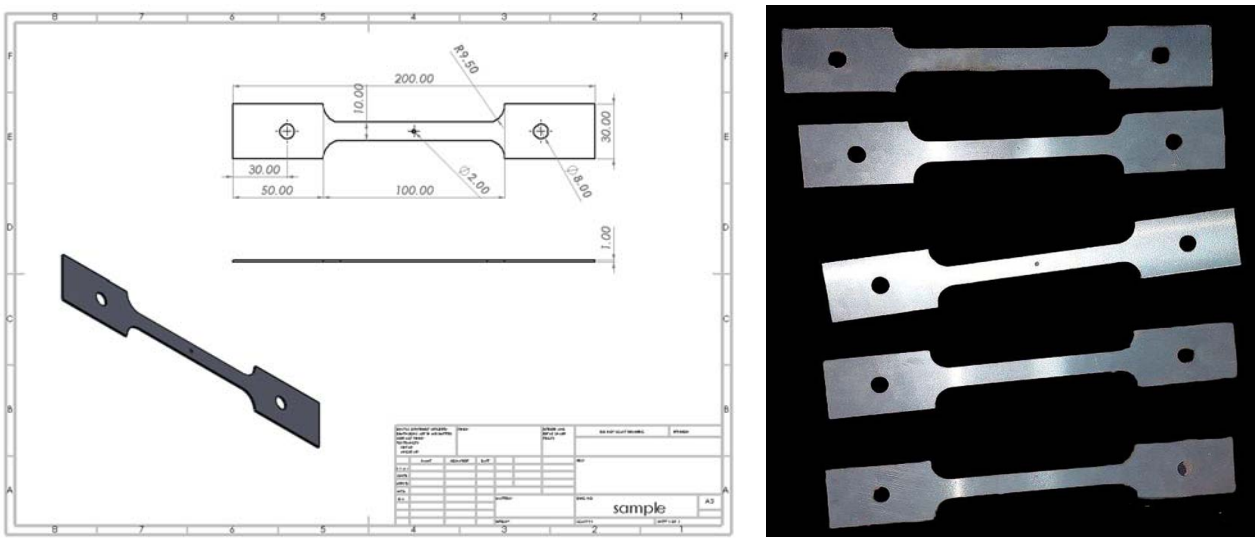


Fig.3. The design and manufactured testing sample.

## 5. Thermal shock testing process

The operation of the testing rig can be described through fixing the tested sample to the upper frame fixture, passing inside the heaters and connected with a weight scale at the lower fixture. Then, the sample is loaded mechanically by pulling it through turning the connected screw, making the scale read the desired mechanical applied load to the sample. After the mechanical load is settled, the heaters are operated till the temperature reaches the highest testing value of *200℃*. Few minutes later, after the temperature is settled, the electronic system switches off the heaters using a relay that is controlled by Arduino, which simultaneously operates the air blower to give the cooling shock to the test sample. Where the blower is cooling the sample to the minimum temperature expected of about *50℃* in this experimental work. At the end of this operation, one cycle of heating and cooling is done. During the experimental testing, this cycle will be repeated and counted by the control system according to the number of switches off the air blower, while the temperatures (higher and lower) are measured continuously by using thermocouples fixed near the heater and another at a linear path of the air. Where these thermocouples are connected to the thermal sensors, then to the control system.

Figure 4 shows that the temperature is rising with time until reached *200℃*; it could be more, but experimentally the testing rig is controlled to reach *200℃* as the highest temperature, which is the top of the heating phase of thermal cyclic loading. After that, the cold air is starting to blow and the cooling phase starts; later, the cycle repeats again. The thermal loading cycle shown in Fig.4 illustrates that the overall periodic time for one thermal cycle is *39* sec. The cause of choosing the highest temperature at *200℃* was due to the creep behavior that could occur for the selected aluminum alloy if the temperature goes further based on the relation obtained from Jones [13];

$$T_{creep} = 0.4\,T_{melting}\,. \tag{5.1}$$

Where the melting temperature of the Al metal is *660℃*.
The transient thermal distribution along the plate and particularly at the central hole during heating and cooling phases is recorded to find the thermal loading cycle that is the main cause of fatigue failure. Where repeating this cycle, a crack initiation will occur and absolutely grow with time during the cyclic loading. The experimental tests were made taking into consideration the central hole size as the testing case studies listed in Tab.3. These tests were repeated twice for each hole size sample to confirm the obtained data and get validations of the results with a dispersion of about *3%* that occurred during the settled period of time.

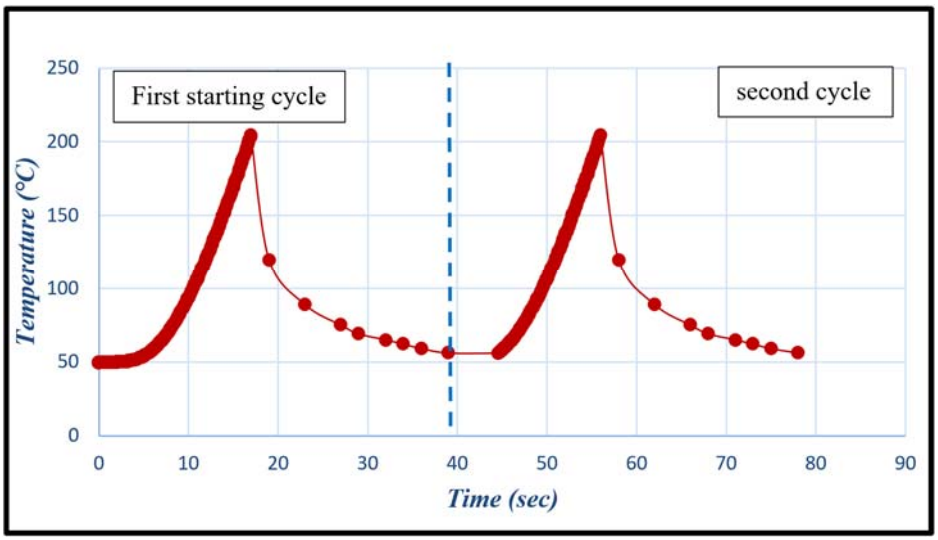


Fig.4. Two thermal cycles during the experimental thermal loading.

Table 3. The test cases of the experimental work.

| Case No. | Hole diameter, *mm* | Temperature range, *℃* | Mechanical load, *kg* |
|---|---|---|---|
| Case No.1 | *1* | *50 - 200* | *200* |
| Case No.2 | *2* | *50 - 200* | *200* |
| Case No.3 | *3* | *50 - 200* | *200* |

## 6. Thermo-mechanical fatigue loading measurements

The determination of the fatigue crack growth rate behavior of an aluminum alloy Al7050 containing different sizes of the central hole is necessarily needed to estimate thermal and mechanical stresses applied to the plates. These stresses are important to translate into combined stress intensity factors at the circumference of the central hole, which is the location of crack initiation. The effective combined stress estimation in this work is divided into mechanical stress obtained from weight load and thermal stress obtained from thermal shock cycling. The calculations of these stresses are as follows:

### 6.1. Thermal stresses

Thermal stress is generated during the repeating of the thermal cycle; the plate is subjected to maximum stress at the highest temperature (*200℃*) and minimum stress at the settled temperature (*50℃*). So, from using Eq.6.1, the thermal stresses estimation was obtained from Ferdinand and Pytel [14], as follows:

$$\sigma_{thermal} = \alpha E \Delta T \tag{6.1}$$

where;

$$\sigma_{th-\max} = \alpha E \Delta T_{\max} = 345.976\, MPa,$$

$$\sigma_{th-\min} = \alpha E \Delta T_{\min} = 86.494\, MPa$$

and $\alpha$ – for (Al 7050-T6 alloy) = $2.36\ e-05\left(1/C\right)$, by Davis [15],
$E$ – for (Al 7050-T6 alloy) = $73.3\ GPa$,
$\Delta T_{max} = 200°C$,
$\Delta T_{\min} = 50°C$

### 6.2. Mechanical stresses

The mechanical load consists of a constant weight subjected to the thin plate. The experimental load was chosen of *200 kg*, which is about *60%* of the yield strength of the tested material; that means the components made of this type of material work under a safety factor of *1.65*. The mechanical stress and safety factors were estimated by Eq.6.2 and Eq.6.3, as in Ferdinand and Pytel [14], and this stress is changed due to the central hole size as shown in Tab.4.

$$\sigma_{mechanical} = \frac{F}{A} = \frac{W \cdot g}{th \cdot \left(w - a\right)}, \tag{6.2}$$

$$n_{safety\ factor} = \frac{\sigma_{yield}}{\sigma_{mechanical}} \tag{6.3}$$

where;

$$W = 200\ kg,\ \ th = 1\ mm,\ \ w = 10\ mm,\ \ a = 1,\ 2,\ 3\ mm.$$

### 6.3. Combined stresses

The interaction effect of combining the mechanical and thermal stresses will behave as an axial stress, where the mechanical stress works as a tensile stress, while the thermal stress works oppositely as a compression stress, and the measurement of the maximum and minimum combination of stresses can be expressed by Eqs. 6.4, 5 and 6, also the stress ratio ($R$), which is the ratio of the minimum stress to the maximum stress as described in Eq.6.7, by Ragab and Bayoumi [16]. The descriptions of the obtained stresses for all the cases are listed in Tab.4.

$$\sigma_{Combined} = \sigma_{Mechanical} - \sigma_{thermal}, \tag{6.4}$$

$$\sigma_{Comb-max} = \sigma_{Mechanical} - \sigma_{ther-min}, \tag{6.5}$$

$$\sigma_{Comb-min} = \sigma_{Mechanical} - \sigma_{ther-max}, \tag{6.6}$$

$$R = \frac{\sigma_{Comb-min}}{\sigma_{Comb-max}}. \tag{6.7}$$

The average combined stress for all hole size cases can be obtained from Ragab and Bayoumi [16] is equal to;

$$\Delta\sigma_{Comb} = \sigma_{Comb-max} - \sigma_{Comb-min} = 259.482\,MPa\,. \tag{6.8}$$

### 6.4. Stress intensity factor

The stress intensity estimation at the sides of the circumference of the central hole in the plate during thermo-mechanical cyclic loading is very necessary. This is crucial to find out the fatigue crack growth rate behaviour for alloy Al7050 plate with this case model. The stress intensity factor depends on many fundamental elements, such as the average stress, the shape of initial cracking in the plate, and the crack length. These factors should be less than the fracture toughness of the design plate.

The measurements of the stress intensity factor for mode I were adopted by Eq.6.9, by Ragab and Bayoumi [16], where the plate is under tensile mode as follows;

$$\Delta K_I = CCF \cdot \Delta\sigma_{Comb} \cdot \sqrt{\pi a} \le \Delta K_{Ic}\,. \tag{6.9}$$

Where; $\Delta K_{Ic}$ is the fracture toughness of the plate, where the critical stress intensity at the beginning (initiation) of the crack as listed in Tab.4 and discussed in Eq.6.10, by Ragab and Bayoumi [16];

$$\Delta K_{Ic} = \Delta\sigma_{Comb} \cdot \sqrt{\pi a}\,. \tag{6.10}$$

CCF is the correction factor of the configuration that depends on the loading and geometry of the cracked body.

For double cracks at a circular hole with radius ($r$), made in the middle of a finite plate, where the CCF factor is described by Eq.6.11, by Ragab and Bayoumi [16];

$$CCF = \left(\frac{r}{a} + 1\right)^{0.5}\,. \tag{6.11}$$

Table 4. The mechanical and combined stresses applied to the thin plate depend on the hole size to width ratio.

| Hole diameter – plate width ratio, (a/w) | Mechanical stresses, $\sigma_{mechanical}\ (MPa)$ | Maximum combined stress $(MPa)$ | Minimum combined stress $(MPa)$ | Stress ratio $R$ | Fracture toughness $\left(MPa \cdot mm^{0.5}\right)$ |
|---|---|---|---|---|---|
| *0.1* | *218* | *131.506(tension)* | *-127.976(compr.)* | *-0.97* | *459.92* |
| *0.2* | *245.25* | *158.756(tension)* | *-100.726(compr.)* | *-0.63* | *650.42* |
| *0.3* | *280.28* | *193.786(tension)* | *-65.696(compr.)* | *-0.34* | *796.6* |

## 7. Results and discussions

The results description is sorted according to different variable relations as follows;

### 7.1. Hole size with crack growth relation

The relation between hole size and crack growth is presented in Fig.5. It is shown that the crack length increased with increasing the number of cycles, and as the hole size increased, the crack growth increased, but in a similar profile. This returned to the fact that thermal cycling on the plate has the same influence and was not affected by the hole size. That means the plates under testing in all cases are suffering the same thermal

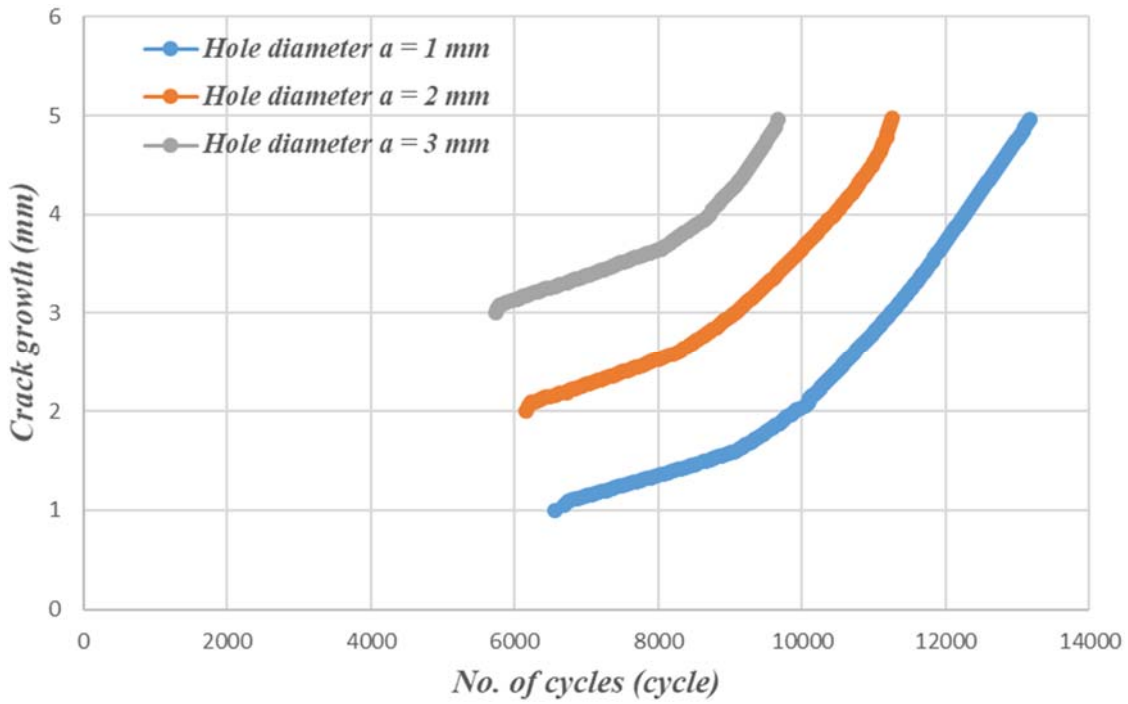


Fig.5. The crack growth relation with No. of cycles for different central hole sizes.

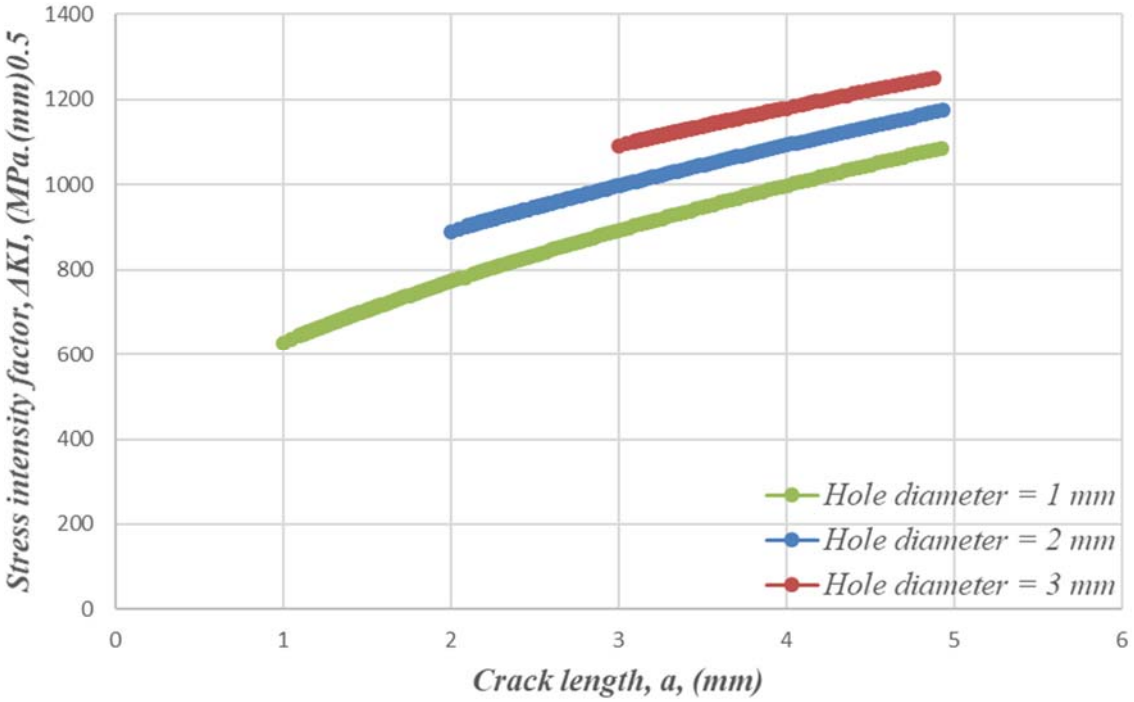


Fig.6. The stress intensity relates to crack length for different central hole sizes.

stress, but because there is a constant mechanical load applied on the plates, the combined stress changes depending on the hole diameter, which reduces the plate width when it is increased. In addition, high temperature reduced the alloy strength limits indicated by yield or ultimate stresses. Therefore, this strength reduction and increased hole diameter under the same applied mechanical load make the plate fracture faster,

as shown in the comparison between the curves in Fig.5. Also, showing that when the crack length plus the hole diameter reach about (*5 mm*), the plate is fractured for all cases; for this, the maximum crack growth is limited by this value based on thermo-mechanical loading conditions of the test.

The relation between the hole size and crack growth shows that, when the central hole diameter increased, the crack initiation started earlier and the crack growth increased and goes faster. This is based on the stress concentration on the sides of the hole circumference parallel to the edges of the thin plate.

### 7.2. Stress intensity and crack length relation

The importance of this factor is related to the information given on the intensity of the stresses concentrated at the tip of a crack during growth. The relation between the crack length and stress intensity factor is directly as shown in Fig.6. When the crack length increased, which means growth, the intensity factor increased too. The increment of the hole size increased the stress intensity. This is due to the effect of hole diameter on the mechanical stress obtained in the thin plate, also on the crack initiation where the crack started from.

### 7.3. Crack growth to No. of cycles rate with stress intensity relation

The crack growth rate with the number of cycles related to the stress intensity for different hole sizes is shown in Fig.7. These relations present three regions, where the discussion is based on these regions as follows:

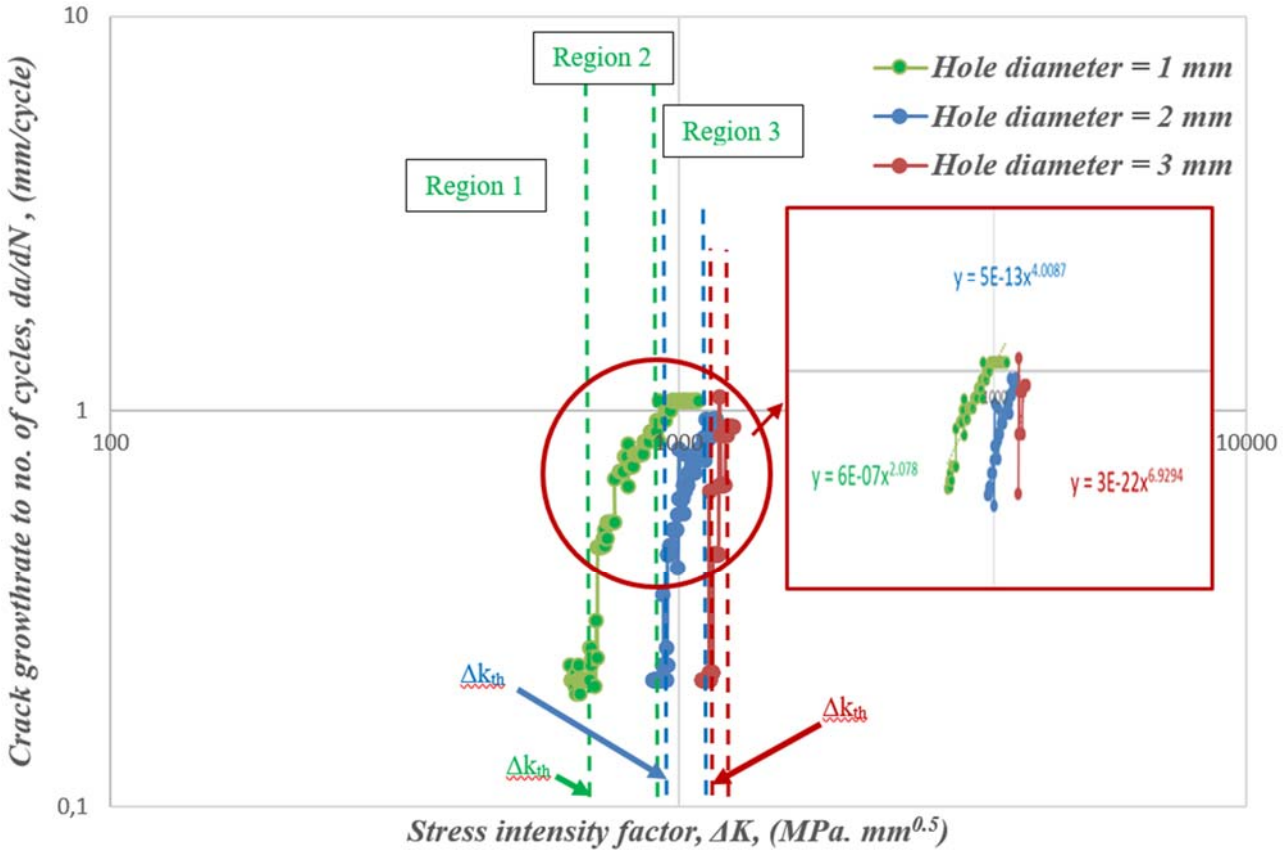


Fig.7. The crack propagation rate to No. of cycles related to stress intensity under different hole sizes.

I. The first region, where there is no observation of crack occurrence, started with threshold stress intensity range value $(\Delta K_{th})$. According to the presented results, the threshold values increased with increasing

the hole size based on thermo-mechanical cyclic loading, material properties and testing conditions as listed in Tab.5.
The crack initiation can be identified experimentally based on the observation and measurements of the crack length that were made periodically within *15* minutes during the test operation. While the threshold value expressed based on the recorded data in Paris low graphs as shown in Fig.7, which is the vertical line passing through the initial points and crossed with the inclined line passing through the crack propagation data. This vertical line indicated the main value of the threshold limit for each hole size and varied accordingly, making the initiation earlier.

Table 5. The threshold stress intensity factors for different hole size cases.

| Hole diameter $a\,(mm)$ | Threshold stress intensity factor $\left(MPa\cdot mm^{0.5}\right)$ | No. of thermal fatigue cycles (cycle) |
|---|---|---|
| *1* | *729.71* | *8920* |
| *2* | *960.751* | *8292* |
| *3* | *1148.35* | *7980* |

II. The second region is the steady crack propagation or growth. It has a linear relationship when the data graph is on a logarithmic scale; for this, the relation between the crack growth to the number of cycle rates with the stress intensity factor can be empirically related by an equation called the Paris law as in Eq.7.1 [16]:

$$\frac{da}{dN}=C\left(\Delta K\right)^{m}. \tag{7.1}$$

Where; $C$ and $m$ are constants that are mainly measured depending on the material properties and testing operating conditions, such as temperature, stress range, stress cycling frequency, and environment. The magnitude of $C$ is determined when the value of $\left(da/dN\right)$ related to $\Delta K$ equals *1* $\left(MPa\cdot mm^{0.5}\right)$ and $m$ is the slope of the data line passing through the points in this region.

Table 6. The Paris law constants for crack growth rate regions for different hole size cases.

| Hole diameter *a (mm)* | $C$ – constant $\left(MPa\cdot mm^{0.5}\right)$ | $m$ – constant |
|---|---|---|
| *1* | *6 e-7* | *2.078* |
| *2* | *5 e-13* | *4.0087* |
| *3* | *3 e-22* | *6.9294* |

The presented results show that this region is changed according to the hole size, so the length of this region decreased when the hole size increased, and with it the slope changed also. The values of the experimental constraints of Paris law for each test case are listed in Tab.6.

According to the constants, there is a large variation in data, especially for the $C$ constant. This is related to the deep impact of the hole size on the crack propagation over a period of time under cyclic loading, which means as the hole size increases, the crack propagation goes faster. Unfortunately, there isn't any precedent literature similar to this concept of work and type of material, making it difficult to present a confidence level for these Paris law constants depending on the hole size. But, depending on the twice repetitions of the tests for each hole size sample, the statistical error obtained was *7.8%*.

This region is very important in fracture mechanics theory because it gives clear information about the behavior of the selected aluminum alloy 7050-T6 in this experimental work under the same geometrical model

and testing thermo-mechanical cyclic loading. So that, from the Paris laws (constants) of the aluminum alloy 7050 for different central hole sizes, it can be easily informed and analyzed the behavior of any engineering structure made of this type of material under the same loading conditions and predict its fracture behavior or failure limits or fatigue lives.

Accordingly, the obtained Paris laws under the mentioned experimental operating condition that is nearly close to the operation of an automotive engine piston or cylinder head made of this type of material. This can be used precisely to predict its thermo-mechanical fatigue life under different geometrical shapes containing the same sizes of holes, defects, cavities, or without.

III. The third region, where the crack growth rate is unstable, leads to extremely harmful and fast fractures. The crack length in this region reached the critical limit of size just before the fracture. From an engineering point of view, this crack length is correlated with the end of the second region. Where, this crucial crack length value can be used to determine or numerically predict the safe life of any engineering structure subjected to fatigue loading.

In this presented work, this region is very short for all cases as shown in Fig.7, due to the significant decay of the alloy strength properties under high temperature and fast failure of testing samples.

## 8. Conclusion

The conclusions of this work are briefly summarized as follows:

1. The crack length increased with increasing the number of thermal cycles, and as the hole size increased, the crack growth increased within a similar profile.
2. When the central hole diameter increased, the crack initiation started early and the crack growth increased, then went faster; this is based on the stress concentration occurring in the hole circumference edges.
3. The increment of the hole size increased the stress intensity, due to the effect that the hole diameter maximized the mechanical stress obtained in the thin plate.
4. The threshold stress intensity increased with increasing the hole size, this is dependent on thermo-mechanical cyclic loading, material properties and testing conditions.
5. The length of the second region decreased when the hole size increased and its slope changed too. For that, different Paris laws were obtained depending on the hole size.
6. The obtained Paris laws under the experimental operating condition can be used precisely to predict the thermo-mechanical fatigue life of an automotive engine piston or cylinder head made of this type of material under different geometrical shapes containing the same sizes of holes, defects, or cavities.
7. The third region is very short for all cases due to the significant decrease in the alloy strength property under high temperatures and catastrophic fractures.

## Nomenclature

$a$ – central hole diameter, *mm*
$C$ – constant.
$CCF$ – the configuration correction factor
$da/dn$ – the ratio of crack length to the No. of cycles, *mm/cycle*
$E$ – elastic modulus of elasticity, *GPa*
$m$ – constant
$N$ – number of cycles, cycle
$R$ – stress ratio.
$T_{creep}$ – creep temperature, *°C*
$T_{melting}$ – melting temperature, *°C*
$th$ – plate thickness, *mm*
$W$ – constant applied weight, *kg*
$w$ – plate width, *mm*

$\alpha$ – linear thermal expansion coefficient, $1/°C$

$\Delta K_I$ – tensile stress intensity factor at the crack starting from the hole edge, $MPa \cdot mm^{0.5}$

$\Delta K_{IC}$ – fracture toughness of the plate, which is the critical stress intensity at the initiation of the crack, $MPa \cdot mm^{0.5}$

$\Delta K_{th}$ – threshold stress intensity range, $MPa \cdot mm^{0.5}$

$\Delta T_{max}$ – maximum temperature range, $°C$

$\Delta T_{min}$ – minimum temperature range, $°C$

$\Delta\sigma_{Comb}$ – combined stress range, $MPa$

$\sigma_{Combined}$ – combined stress, $MPa$

$\sigma_{Comb-max}$ – maximum combined stress, $MPa$

$\sigma_{Comb-min}$ – minimum combined stress, $MPa$

$\sigma_{Mechanical}$ – mechanical stress, $MPa$

$\sigma_{th-max}$ – maximum thermal stress, $MPa$

$\sigma_{th-min}$ – minimum thermal stress, $MPa$

## References

[1] Ali M.A., Hasan S.T. and Myriounis D.P. (2012): *A method of analysis to estimate thermal down-shock stress profiles in hollow cylinders when subjected to transient heat/cooling cycle.*– Advanced Materials Research, vol.445, pp.893-898, DOI: 10.4028/scientific5/AMR.445.893.

[2] Garden C.A., Mc Evily A.J. and Wells C.H. (1973): *Fatigue at elevated temperature.*– American Society for Testing and Materials, ASTM STP 520.

[3] Szmytka F., Salem M., Rezai-Aria F. and Oudin A., (2015): *Thermal fatigue analysis of automotive Diesel piston: Experimental procedure and numerical protocol.*– International Journal of Fatigue, vol.73, pp.48-57, DOI: 10.1016/J.IJFATIGUE.2014.11.011.

[4] Muthukumaran R., Daniel A.A., Nithya M., Parthiban A., Sathish T., Giri J. and Al-Lohedan H.A. (2024): *Characterization on properties of Al7050/TiC/BN hybrid metal matrix composite.*– AIP Advances, vol.14, No.045318, DOI: 10.1063/5.0204280.

[5] Abo El-Nasr A., Ayad M. and Fattouh M. (2002): *High temperature fatigue behavior of 7075Al via low plasticity burnishing.*– Engineering Research Journal, vol.25, No.2, DOI: 10.21608/erjm.2002.70750.

[6] Chaussumier M., Mabru C., Chieragatti R, and Shahzad M. (2013): *Fatigue life model for 7050 chromic anodized aluminium alloy.*– Procedia Engineering, vol.66, pp.300-312, DOI: 10.1016/j.proeng.2013.12.085.

[7] Engler-Pinto Jr. C.C., Lasecki J.V., Boileau J.M. and Allison J.E. (2004): *A comparative investigation on the high temperature fatigue of three cast aluminum alloys.*– SAE International Technical Paper Series, DOI: 10.4271/2004-01-1029.

[8] Liu K., Wang S., Pan L. and Chen X.-G. (2023): *Thermo-mechanical fatigue behavior and resultant microstructure evolution in Al-Si 319 and 356 cast alloys.*– Materials, vol.16, No.2, p.829, DOI: 10.3390/ma16020829.

[9] Mahan H.M., Konovalov S.V., Najm S.M., Oleksik M. and Trzepieciński T. (2024): *Experimental and numerical investigations of the fatigue life of AA2024 aluminium alloy-based nanocomposite reinforced by TiO2 nanoparticles under the effect of heat treatment.*– International Journal of Precision Engineering and Manufacturing, vol. 5, pp.141-153, DOI: 10.1007/s12541-023-00906-4.

[10] Abdallah S., Mohamed E., and El-Amine Slimani M. (2019): *Crack growth study under thermo-mechanical loads: parametric analysis for 2024 T3 aluminum alloy.*– Frattura ed Integrità Strutturale, vol.13, No.50, pp.235-245, DOI: 10.3221/IGF-ESIS.50.19.

[11] Hussain F., Abdullah S. and Nuawi M.Z. (2016): *Effect of temperature on fatigue life behaviour of aluminium alloy AA6061 using analytical approach.*– Journal of Mechanical Engineering and Sciences (JMES), vol.10, No.3, pp.2324-2235, DOI: 10.15282/jmes.10.3.2016.10.0216.

[12] Kadhim M.J. and Kamal H.M. (2018): *cumulative thermal fatigue damage for aluminum alloy under variable stresses.*– International Conference on Materials Engineering and Science, IOP Conf. Series: Materials Science and Engineering, vol.454, No.1, p.012145, DOI: 10.1088/1757-899X/454/1/012145.

[13] Jones R.M. (1998): *Mechanics of Composite Materials*.– Second Edition Professor of Engineering Science and Mechanics Virginia Polytechnic Institute and State University Blacksurg, Virginia, 24061-0219.

[14] Singer F.L. and Pytel A. (1980): *Strength of materials*.– third edition, Harper and Row, publishers, New York.

[15] Davis J.R. (2001): *Aluminum and aluminum alloys*.– Alloying: Understanding the Basics, ASM International, pp.351-416.

[16] Ragab A. and Bayoumi S. (1998): *Engineering Solid Mechanics*.– CRC press, p.994.

Received: June 3, 2025
Revised: December 12, 2025